

# Specimen alignment with limited point-based homology: 3D morphometrics of disparate bivalve shells (Mollusca: Bivalvia)

Stewart M Edie  $^{\text{Corresp., 1}}$ , Katie S Collins  $^{2}$ , David Jablonski  $^{3,4}$ 

Corresponding Author: Stewart M Edie Email address: edies@si.edu

Comparative morphology fundamentally relies on the orientation and alignment of specimens. In the era of geometric morphometrics, point-based homologies are commonly deployed to register specimens and their landmarks in a shared coordinate system. However, the number of point-based homologies commonly diminishes with increasing phylogenetic breadth. These situations invite alternative, often conflicting, approaches to alignment. The bivalve shell (Mollusca: Bivalvia) exemplifies a homologous structure with few universally homologous points—only one can be identified across the Class, the shell 'beak.' Here, we develop an axis-based framework, grounded in the homology of shell features, to orient shells for landmark-based, comparative morphology. As the choice of homologous points for alignment can affect shape differences among specimens, so can the choice of orientation axes. Analysis of forty-five possible alignment schemes finds general conformity among the shape differences of 'typical' equilateral shells, but the shape differences among atypical shells can change considerably, particularly those with distinctive modes of growth. Each alignment implies a hypothesis about the ecological, developmental, or evolutionary basis of morphological differences, but we recognize one alignment in particular as a continuation of the historical approaches to morphometrics of shell form: orientation via the hinge line. Beyond bivalves, this axis-based approach to aligning specimens facilitates the comparison of continuous differences in shape among many other phylogenetically broad and morphologically disparate samples.

<sup>1</sup> Department of Paleobiology, National Museum of Natural History, Smithsonian Institution, Washington, DC, United States

Department of Earth Sciences, Invertebrates and Plants Palaeobiology Division, Natural History Museum, London, United Kingdom

<sup>&</sup>lt;sup>3</sup> Department of the Geophysical Sciences, University of Chicago, Chicago, IL, United States

<sup>&</sup>lt;sup>4</sup> Committee on Evolutionary Biology, University of Chicago, Chicago, IL, United States



- 1 TITLE: Specimen alignment with limited point-based homology: 3D morphometrics of
- 2 disparate bivalve shells (Mollusca: Bivalvia)
- 3 **RUNNING HEAD:** Aligning bivalve shells
- 4 **KEYWORDS:** marine bivalve, shell shape, geometric morphometrics, 3D morphometrics,
- 5 anatomical homology
- 6 **AUTHORS:** Stewart M. Edie<sup>1\*</sup>, Katie S. Collins<sup>2</sup>, David Jablonski<sup>3,4</sup>
- 7 Department of Paleobiology, National Museum of Natural History, Smithsonian Institution,
- 8 Washington, DC, 20013, U.S.A.
- 9 <sup>2</sup> Natural History Museum, London, London, SW7 5BD, United Kingdom
- 10 <sup>3</sup> Department of the Geophysical Sciences, University of Chicago, 5734 South Ellis Ave,
- 11 Chicago, IL 60637, USA.
- 12 <sup>4</sup> Committee on Evolutionary Biology, University of Chicago, Chicago, IL 60637, USA
- \* corresponding author

#### 14 1. Abstract

- 15 Comparative morphology fundamentally relies on the orientation and alignment of specimens. In
- 16 the era of geometric morphometrics, point-based homologies are commonly deployed to register
- 17 specimens and their landmarks in a shared coordinate system. However, the number of point-
- 18 based homologies commonly diminishes with increasing phylogenetic breadth. These situations
- invite alternative, often conflicting, approaches to alignment. The bivalve shell (Mollusca:
- 20 Bivalvia) exemplifies a homologous structure with few universally homologous points—only
- one can be identified across the Class, the shell 'beak.' Here, we develop an axis-based
- framework, grounded in the homology of shell features, to orient shells for landmark-based,
- 23 comparative morphology. As the choice of homologous points for alignment can affect shape
- 24 differences among specimens, so can the choice of orientation axes. Analysis of forty-five
- 25 possible alignment schemes finds general conformity among the shape differences of 'typical'
- 26 equilateral shells, but the shape differences among atypical shells can change considerably,
- 27 particularly those with distinctive modes of growth. Each alignment implies a hypothesis about
- 28 the ecological, developmental, or evolutionary basis of morphological differences, but we
- 29 recognize one alignment in particular as a continuation of the historical approaches to
- morphometrics of shell form: orientation via the hinge line. Beyond bivalves, this axis-based
- 31 approach to aligning specimens facilitates the comparison of continuous differences in shape
- 32 among many other phylogenetically broad and morphologically disparate samples.



#### 2. Introduction

- 34 Comparative morphology depends on how organisms are oriented, or aligned. For a simplistic
- example, a kiwi's beak is relatively long for a bird when measured from the tip to the base of the
- 36 skull, but rather short when measured from the tip to the nostrils (an alternative definition of
- beak length; Borras et al. 2000). Thus, the choice of anatomical reference points can profoundly
- 38 alter our interpretations of evolutionary morphology. Alignments commonly use point-based
- 39 aspects of homologous features—the junction of the kiwi's beak with the cranium (a Type I
- 40 landmark; Bookstein 1992) and the distal-most point of the beak, the tip (a Type III landmark).
- 41 Closely related organisms tend to have more of these homologous points, allowing for a
- 42 straightforward alignment and comparison of their shapes. Alignment on strict, point-based
- 43 homology becomes more problematic with increasing phylogenetic distance, however, as the
- 44 number of homologous features invariably diminishes (Bardua et al. 2019).

Bivalve mollusks have become a model system for macroevolution and macroecology

46 (Jablonski et al. 2017; Edie et al. 2018; Crame 2020), but their strikingly disparate body plans

- 47 complicate Class-wide morphologic comparisons using strict homology (Cox et al. 1969).
- 48 Inimical to triangulation and thus alignment via landmarks, the valve of the bivalve shell—the
- 49 most widely available feature of the animal today and through the fossil record—has only one
- 50 homologous *point*: the apex of the beak, which is the origin of growth of the embryonic shell at
- 51 the apex of the beak (Carter et al. 2012:21; Figure 1). Homology-free approaches can be useful
- 52 for comparing the shapes of shell valves when anatomical orientation is either unknown or
- uncertain (Bailey 2009); but wholesale substitution of shape, i.e. analogy, for homology
- 54 complicates the evolutionary interpretation of morphological differences. Despite the lack of
- 55 multiple homologous *points* on the shell valve across the Class, a number of its *features* are
- homologous and can facilitate comparisons. Here, we apply principles of bivalve comparative
- morphology to develop a framework for aligning shell valves (hereafter 'shells') across the Class,
- thus enabling phylogenetically extensive analyses of their shapes using geometric morphometrics
- despite the remarkable range of body plans across the clade.

### 60 **2.1** Approaches to orienting the bivalve shell



- Many body directions, axes, lines, and planes have been defined for bivalves (see Cox et al.
- 62 1969; Bailey 2009; Carter et al. 2012)—some related to features of the shell (an accretionary
- exoskeleton composed of calcium carbonate; Marin et al. 2012), and others to features of the soft
- body (the digestive tract, foot, byssus, muscles, etc.). Separation into these 'shell' and 'body'
- 65 terms is a false (Stasek 1963a), but convenient dichotomy (Yonge 1954): the shell is generated
- by, and remains attached to, the soft body, but their morphologies can become decoupled (Yonge
- 67 1954; Edie et al. 2022). Still, both shell and body features are required for orientation via
- 68 homology (Stasek 1963*a*; cf. Bailey 2009). Given our goal of aligning the shell for geometric



- 69 morphometrics across broad phylogenetic scales and through the fossil record, we focus on
- orientations that can be inferred from this part alone, but we must use a critical body axis to fully
- 71 determine orientation, the anteroposterior axis. Thus, shell features used for alignment can be
- divided into two classes: (1) intrinsic characteristics of the shell relating to its geometry, growth,
- and biomechanics, and (2) proxies of the body recording the positions of the soft anatomy
- 74 including the adductor muscle scars, pallial line, byssal notch, pedal gape, siphon canal, and
- 75 more.

#### 2.1.1 Orientation via intrinsic characteristics of the shell

- 77 Although the only homologous point on the shell across all bivalves is the apex of the beak
- 78 (hereafter 'beak', Figure 1), aspects of the shell's biomechanics, such as its hinge axis, and its
- 79 accretionary growth permit orientation via homology. The planes and lines proposed to describe
- shell geometry and growth have been criticized for their lack of homology (Stasek 1963b:226)
- and ubiquity across the class (Lison 1949:62; Owen 1952:149; Carter 1967:272). We discuss two
- 82 such features here, the directive plane and demarcation line (Figure 1 and defined below), but we
- 83 also address and test two alternative means of orienting shells that combine the shell's geometry
- 84 and growth: the maximum growth axis and the shape of the shell commissure.
- Related to the shell's biomechanics, the hinge has been treated as a "fixed dorsal region"
- 86 (Yonge 1954:448; see also Jackson 1890:282), later redefined to reflect the position of the
- 87 mantle isthmus bridging between the two valves as a universally dorsal-directed feature (Cox et
- al. 1969:79). Beyond its determination of dorsoventral directionality, the hinge, specifically the
- 89 hinge axis defined as the "ideal line drawn through the hinge area, and coinciding with the axis
- 90 of motion of the valves" (Jackson 1890:309), is a Class-wide feature that can constrain one of the
- 91 three Cartesian axes required for alignment. In a strictly mechanical sense, the ligament, and not
- 92 the hinge teeth, directs the orientation of the axis of motion (Trueman 1964:56; Cox et al.
- 93 1969:47; Stanley 1970:47). However, the hinge area, which includes the teeth, is hypothesized to
- 94 be analogous in function (Cox et al. 1969:47)—guiding the two valves into alignment during
- 95 closure—and homologous in its origin (Scarlato and Starobogatov 1978; Waller 1998; Fang and
- 96 Sanchez 2012). Thus, our definition of the **hinge line** indicates the longest dimension of the
- 97 hinge area (see 'hinge' in Carter et al. 2012:74 and Figure 1); for quantitatively aligning shells,
- 98 the hinge line is determined by the two farthest apart articulating elements of the hinge area,
- 99 excluding lateral teeth, which are variably present among heterodont species (e.g. Mikkelsen et
- al. 2006:493; Taylor and Glover 2021); definition proposed here is a synthesis of the discussions
- in Cox et al. 1969:81 and Bradshaw and Bradshaw 1971). Thus, by directing the orientation of
- the horizontal plane which divides the body into dorsal (towards the beak) and ventral (towards
- the free edge of the shell) territories, the hinge line can also proxy the anteroposterior axis
- 104 (Figure 1, Cox et al. 1969:81 and discussion below).



106

107

108

109

110

111112

113

114

115

116

117

118

119120

121

122

123

124

125

126

127

128129

130

131

132

133134

135

136

137

138139

140141

Related to the geometry and growth of the shell, the **directive plane** (Lison 1949) was proposed as the only plane passing through the shell that contains the logarithmic planispiral line connecting the beak to a point on the ventral margin (Figure 1); all other radial lines would be logarithmic turbinate spirals (or 'helicospirals'; Stasek 1963b:217). In other words, on a radially ribbed shell, there may be a single rib that lies entirely on a plane when viewed from its origin at the umbo to its terminus on the ventral margin; that plane is orthogonal to the commissural plane for planispiral shells (e.g. many Pectinidae, Figure 1), but lies at increasingly acute angles to the commissural plane with increasing tangential components of growth (i.e. geometric torsion; see the trace of the directive plane on *Chione* in Figure 1 and examples in Cox et al. 1969:86-Figs. 70-71). In theory, the directive plane could be used to orient the dorsoventral axis of the shell, but in practice, the feature is not universal across shell morphologies (e.g. the strongly coiled Glossus humanus [as Isocardia cor] in Lison 1949:62; Owen 1952:149). Cox et al. (1969:87) also remark that the plane cannot "be demonstrated easily by visual inspection if the shell lacks radial ribbing, except in rare specimens with an umbonal ridge that proves to lie within the directive plane." Difficulty in application is no excuse to avoid an approach, but the nonuniversality of this feature renders it inapplicable to Class-wide comparisons of shell shape.

Owen (1952) proposed an alternative to the directive plane: the **demarcation line** (Figure 1; originally termed the 'normal axis' but re-named by Yonge 1955:404). As with the directive plane, the demarcation line serves to orient the dorsoventral direction and separate the shell into anterior and posterior 'territories' (Yonge 1955:404; Morton and Yonge 1964:40), but its definition has been variably characterized in geometric and/or anatomical terms. Per Owen (1952:148), the demarcation line can "be considered with reference to three points: the umbo, the normal zone of the mantle edge and the point at which the greatest transverse diameter of the shell intersects the surface of the valves." Yonge (1955:404), acknowledging correspondence with Owen, described the demarcation line as: "the projection onto the sagittal plane of the line of maximum inflation of each valve ... starting at the umbones. ... i.e. the region where the ratio of the transverse to radial component in the growth of the mantle/shell is greatest." Carter et al. (2012:52) provided perhaps the clearest description as the line defining the "dorsoventral profile when the shell is viewed from the anterior or posterior end." However, Stasek (1963b) demonstrated the difficulty in measuring this line; note the nearly orthogonal orientations of the empirically determined demarcation line on *Ensis* (Stasek 1963b:225-Fig.5a) compared to its initially proposed position (Owen 1952:148-Fig. 5). Stasek's empirical approach, coupled with the revised definition of Carter et al., is tractable with today's 3D-morphology toolkit. But, critically, this definition depends on the direction of the anteroposterior axis, which itself is variably defined (see discussion in next section). Thus, definitionally driven shifts in the direction of the anteroposterior axis can alter the trace of the demarcation line. Owen's initial definition is independent of the anteroposterior axis, but as Stasek demonstrated, its



identification can be unreliable. Thus, high degrees of digitization error for the demarcation line may confound comparisons of shell shape, and we do not include the demarcation line as a feature for aligning shells across the Class.

Both the directive plane and the demarcation line attempt to orient the shell on aspects of its geometry that are intrinsic to its growth. A similar and more reliably determined approach may be orientation to the **maximum growth axis** (i.e. **line of greatest marginal increment** sensu Owen 1952; Figure 1). The maximum growth axis is the straight line that connects the origin and terminus of the trace of maximum growth across the shell surface. This trace connects the beak to the ventral margin along a perpendicular path to the most widely spaced commarginal growth increments (as such, this definition appears to have similar properties to the trace of the directive plane on the shell surface). But, as for the directive plane and the demarcation line, the maximum growth axis can be prone to measurement error without fitting a formal model of shell growth (e.g. those of Savazzi 1987; Ubukata 2003), and should therefore be used with caution. However, a reasonable and reliably measured proxy for this axis is the line lying on the commissural plane that originates at the beak and terminates at the furthest point on the shell commissure. Thus, this axis can indicate the dorsoventral orientation of the shell.

Orientation using the **shape of the shell commissure** offers, arguably, the most reliably determined approach that uses intrinsic properties of the shell (Figure 2a). Given the accretionary growth of the shell, points on the commissure—the homologous leading edge of shell growth (Vermeij 2013)—are geometrically homologous, or correspondent (Bookstein 1991; Gunz et al. 2005). Valve handedness is still required to ensure that compared valves are from the same side of the body (i.e. left vs. right), which requires anteroposterior directionality (see below). This alignment thus orients shells using geometric correspondence based on homology of growth.

The sagittal axis is crucial to the shell's three-dimensional alignment and is likely the least controversially defined. This axis is the pole (=normal) to the sagittal plane, which lies parallel to the commissural plane defined as: "the more proximal part of the line or area of contact of the two shell valves" (Carter et al. 2012:38). Therefore, the sagittal axis is parallel to the frontal and horizontal planes (Figure 1). The proximal direction is towards the commissural plane and the distal direction is towards the shell's summit: the point on the shell that is maximally distant from the commissural plane (Figure 1, Cox et al. 1969:108; Carter et al. 2012:177). If valve handedness (i.e. left vs. right laterality) and the directionality of the dorsoventral and anteroposterior axes are known, then this axis is rarely required for orientation. However, certain definitions of the anteroposterior and dorsoventral axes are not constrained to be orthogonal (e.g. in monomyarian taxa with the anteroposterior axis defined as the oro-anal axis, see below, and the dorsal ventral axis as the axis of maximum growth—*Pecten* in Figure 1); as the axes representing the anteroposterior and dorsoventral directions become more parallel,



196

197

198

199

200

201

202

203204

205

206

207

208

209

210

211

then the sagittal axis becomes an increasingly important safeguard against the inversion of the

proximal-distal direction in quantitative alignments.

#### 2.1.2 Orientation via the soft-body as reflected on the shell

181 Anteroposterior directionality is the third Cartesian axis required for orienting the bivalve shell 182 in three-dimensions. The positions of the mouth (anterior) and anus (posterior) ultimately determine the anteroposterior axis (Jackson 1890, 'preferably' described as the 'oro-anal' axis in 183 Cox et al. 1969:79), but the exact positions of these two soft-body features are rarely recorded 184 directly on the shell. Thus, tactics for determining the polarity, if not the precise bearing, of the 185 186 anteroposterior axis have relied on lineage or body-plan specific proxies—shell features that are 187 assumed to correlate with positions of the soft-body anatomy (e.g. positions of the adductor muscle scars, Figure 1a, Cox et al. 1969:79). Disparate body plans necessitate taxon-specific 188 189 rules for orientation, such that determining the anterior and posterior ends of the shell requires a mosaic approach. For example, there are at least three definitions of the anteroposterior axis in 190 191 dimyarians alone (Bailey 2009:493), which necessarily differ from those of monomyarians considering the reliance on two, instead of one, adductor muscle scars. For those monomyarians, 192 which commonly have lost the anterior adductor (Yonge 1954; but see loss of the posterior 193 194 adductor in the protobranch Nucinellidae, Allen and Sanders 1969; Glover and Taylor 2013), 195 additional shell features are used to orient the anteroposterior axis. In pectinids, the byssal notch

Lineage or body-plan specific definitions help with anteroposterior orientation of shells that lack point-based homology (e.g. two muscle scars vs. one), but they still rely on proxies for the position of soft-body features that may not be determined for taxa known only from their shells, e.g. some fossils (Bailey 2009). Hypothesizing anteroposterior orientation using phylogenetic proximity to extant clades may help, but this approach should be used with caution in given the lack of direct anatomical evidence—especially when phylogenetic affinities are either unknown or distant, as for many Paleozoic taxa (Bailey 2009). Nor is it advisable to assume the precise bearing of the anteroposterior axis is identical to another, well-defined axis, such as the hinge line (see variable bearings of the anteroposterior axis and hinge *axis* in Cox et al. 1969:80-Fig. 64). However, if the phylogenetic or temporal scope of an analysis precludes the determination of the anteroposterior axis using homologous body features with geometric correspondences (e.g. inclusion of dimyarian and monomyarian taxa), then the hinge line offers a universal proxy; that way, multiple features can be used to determine the anterior and posterior ends of the shell (Cox et al. 1969).

of the anterior auricle proxies the location of the mouth (Figure 1b), but in ostreids, the mouth is

more centrally located under the umbo, near the beak (Yonge 1954:448).



224225

226

227228

229

230

231

232233

234

235

236

237

238

239

240

241

242

243

244

#### 212 2.2 Alignment of shells for geometric morphometrics

- 213 Our challenge here is to reconcile the many means of orienting bivalve shells discussed above
- 214 into alignment schema for geometric morphometrics. We compare the differences in shell shape
- 215 produced by the five orientations listed below. All five orientations use the sagittal axis (SX) to
- 216 determine the lateral orientation of the shell. Precise definitions of landmark placement for each
- 217 axis are provided in the Methods.
- **SX-HL-oHL.** Anteroposterior orientation determined by the hinge line (HL); dorsoventral orientation determined by the orthogonal line to the HL within the commissural plane (oHL). This alignment emulates the orientation scheme for measuring shell height, length, and width—the most common and widely applicable framework for comparing shell morphology (Cox et al. 1969:81–82; Kosnik et al. 2006).
  - **SX-OAX-oOAX.** Anteroposterior orientation determined by the proxied positions of the mouth and anus using shell features (oro-anal axis, OAX); dorsoventral orientation determined by the orthogonal line to the OAX within the commissural plane (oOAX). Similar to SX-HL-oHL, this alignment largely determines orientation by a single axis, the OAX, which has also been used to frame linear measurements of shell morphology (e.g. Stanley 1970:19).
  - **SX-HL-GX.** Anteroposterior orientation determined by the hinge line (HL); dorsoventral orientation determined by the maximum growth axis (GX). This alignment allows an aspect of shell growth to affect its orientation and thus the degrees of morphological similarity among specimens.
  - **SX-HL-GX-OAX.** Anteroposterior orientation determined by the directions of both the HL and OAX; dorsoventral orientation determined by GX. This 'full' alignment scheme allows axes derived from intrinsic characteristics of the shell and the body to affect orientation.
  - **SX-COMM.** Anteroposterior and dorsoventral orientation determined by the shape of the commissure curve, with the initial point nearest the beak (Figure 2a). This alignment uses the geometric correspondence of semilandmarks on the commissure that capture the relationship between its shape and growth.

Procrustes superimposition (or Procrustes Analysis) is the workhorse of geometric morphometrics—aligning shapes by translation to a common origin, scaling to common size, and rotation to minimize relative distances of landmarks (see variants thereof in Zelditch et al. 2012). While we are most concerned with assessing the effects of rotation using the five alignments described immediately above, choices of translation and scaling can also influence shape

described immediately above, choices of translation and scaling can also influence shape

246 differences. Thus, we consider all combinations of parameter values for each step in the

247 Procrustes Analysis. As there is arguably no objective criterion to determine which alignment



- best suits bivalve shells, we discuss the benefits and drawbacks of each approach and
- 249 quantitatively compare the similarities of resulting alignments. Ultimately, we use this exercise
- 250 to propose a best practice for aligning bivalve shells and comparing their shapes—a process that
- 251 may be of use for workers in other, similarly disparate morphological systems that lack high
- 252 degrees of point-based homology.
- **253 3. Methods**
- 254 **3.1 Dataset**
- We adopt the style of previous approaches to studying bivalve orientation and use a dataset of
- 256 morphological end-members to illustrate the effects of different alignment schemes (e.g. Owen
- 257 1952; Yonge 1954; Stasek 1963a). Eleven species that represent most major body plans were
- selected to proxy the morphological and anatomical disparity across the evolutionary history of
- 259 the Class (Table S1). Bivalves with highly reduced shells or those that form part of a larger
- structure (tubes and crypts) are not directly analyzed here, but we consider their fit to the
- alignments in the Discussion.
- One valve from an adult individual of each species was sampled from museum
- collections (see Acknowledgments). Nine of eleven individuals are equivalve, and because we do
- 264 not examine details of dentition, their left and right valves are operationally mirror images of
- 265 each other. The inequivalve taxa included here (*Pecten*, *Ostrea*) primarily differ in terms of
- 266 inflation (height above the commissural plane); for the purposes of our analysis, the location of
- 267 key features such as the hinge area and adductor muscle scars are similar enough that using
- 268 either valve gives a similar orientation. Valves were scanned using micro-CT at the University of
- 269 Chicago's Paleo-CT facility, and three-dimensional, isosurface, triangular-mesh models were
- 270 created in VG Studio Max and cleaned in Rvcg (Schlager 2017) and Meshmixer. Landmarks
- were placed using 'Pick Points' in Meshlab (Visual Computing Lab ISTI CNR 2019). Meshes,
- 272 landmarks, and code necessary to reproduce the analyses here are provided in the Supplemental
- 273 Material.
- 274 3.2 Aligning bivalve shells in a geometric morphometrics framework
- 275 **3.2.1** Scaling
- 276 Procrustes Analysis scales objects to a common size, and three alternative scalings are
- 277 considered here: (1) the centroid size of the shell (Figure 2b), (2) the centroid size of the
- commissure (Figure 2a), and (3) the volume of the shell. The centroid size of the shell reflects
- 279 the 3D footprint of the shell, and the centroid size of the commissure reflects the size of the
- shell's growth front. Shell volume—the amount of calcium carbonate—may be less correlated



- with shell shape than the other two measures, and may therefore reveal shape differences not
- 282 intrinsically linked to size.

#### **283 3.2.2 Translation**

- After scaling, Procrustes Analysis translates objects to a common origin. Objects are typically
- 285 'centered' by subtracting the centroid of the landmark set (mean X, Y, and Z coordinate values
- per object) from each landmark coordinate, thus shifting the center of each landmark set to the
- origin (X=0, Y=0, Z=0). Three points are considered for translation here: (1) the **beak** (Figure 1),
- 288 (2) the **centroid of the shell** (Figure 2b), and (3) the **centroid of the commissure** (Figure 2a).
- 289 Translation to the beak positions shells onto the homologous point of initial shell growth.
- 290 Translation to the centroids of the shell or its commissure incorporate more information on the
- shape of the shell, with centering on the commissure adding an aspect of homology by
- 292 positioning shells on their growth front. Operationally, Procrustes Analysis translates landmark
- sets to their respective centroids before minimizing their rotational distances, overriding any
- 294 prescribed translations; the three translations above are therefore implemented after the rotation
- step (following the functionality in *Morpho::procSym* Schlager 2017).

#### 296 **3.2.3 Rotation**

- 297 Rotation in Procrustes Analysis orients landmark coordinates to minimize their pairwise sum of
- 298 squared distances. The 5 orientations discussed in the introduction were used for rotation.
- 299 Because Procrustes Analysis uses Cartesian coordinates, two landmarks were placed on the mesh
- 300 surface of a shell to indicate the direction of each axis as described in the subsections below
- 301 (exact placement of landmarks on specimens in Figure S1).

#### 302 Sagittal orientation

- 303 Sagittal axis [SX]. This axis is the pole to the commissural plane (Figure 1). It is determined as
- 304 the average cross product of successive vectors that originate at the centroid of the commissure
- and terminate at semilandmarks on the commissure curve (visualization of fitting the
- 306 commissural plane in Figure S2). The distal direction is towards the exterior surface of the shell
- and the proximal direction is towards the interior surface.

#### 308 Anteroposterior orientation

- 309 Hinge line [HL]. The hinge line is determined by landmarks placed at the two farthest apart
- articulating elements of the hinge area (Figure 1). The landmarks are then designated as being
- anterior or posterior using the available discriminating features on the shell and can thus proxy
- 312 the anteroposterior orientation. While not an 'axis' in the strict anatomical sense, we group the
- 313 hinge line with the other anatomical axes below.



340

- 314 Oro-anal axis [OAX]. The positions of the mouth and anus or proxies thereof are used to orient
- 315 the oro-anal axis and thus the anteroposterior orientation. For dimyarian taxa, anterior and
- posterior ends of the axis are determined by landmarks placed on the dorsal-most edge of the
- anterior and posterior adductor muscle scars (Figure 1a, the 'Type 2 adductor axis' of Bailey
- 318 2009:493 after Stanley 1970:19). For monomyarian taxa that have retained the posterior adductor
- muscle, the centroid of that adductor muscle scar is landmarked as the posterior end of the axis
- and shell features that reflect the position of the mouth are landmarked as the anterior end (e.g.
- 321 the ventral notch of the anterior auricle in pectinids [Figure 1b] or the beak in ostreids, Yonge
- 322 1954). The axis is reversed in monomyarian taxa that have retained the anterior muscle (e.g. the
- 323 protobranch Nucinellidae, Glover and Taylor 2013).

#### **Dorsoventral orientation**

- 325 Maximum growth axis [GX]. The origin of shell growth at the beak is the dorsal landmark on the
- maximum growth axis and the point on the shell commissure with the greatest linear distance to
- 327 the beak is ventral landmark (Figure 1).
- 328 Orthogonal hinge line [oHL]. By definition, the orthogonal line to the HL (oHL) represents the
- dorsoventral axis, with the dorsal-most point nearest the beak.
- 330 Orthogonal oro-anal axis [oAX]. By definition, the orthogonal axis to the OAX (oOAX)
- represents the dorsoventral axis, with the dorsal-most point nearest the beak.

#### 332 Commissure orientation

- 333 The manually placed landmarks on the shell commissure were used to fit a three-dimensional
- spline on which 50 equally spaced semilandmarks were placed in an anterior direction
- 335 (clockwise for left valves when viewed towards the interior surface, counterclockwise for right
- valves). The semilandmark on the commissure curve nearest the beak landmark was selected as
- the initial point (Figure 2a). Semilandmarks were then slid to minimize bending energy and
- reduce artifactual differences in shape driven by their initial, equidistant placement (Gunz et al.
- 339 2005; Gunz and Mitteroecker 2013; Schlager 2017).

#### Standardized axis points

- We observed that variance among specimens in the distances between the axis landmarks
- 342 notably influenced their best-fit orientation in the Procrustes Analysis (see difference in spacing
- of these landmarks in Figure S1). To remove this 'Pinocchio effect' (sensu Zelditch et al.
- 344 2012:67), axis landmarks were 'standardized' (visualization of this process in Figure 3). The
- vector defined by the two axis landmarks was shifted to the centroid of the shell commissure and
- normalized to unit length; the standardized axis points (we explicitly avoid calling them
- landmarks) were then designated by the terminal points of the unit vector and its negative.



361

363

364

365

366

367

368

369370

371

372

373374

375

376

377

378

379

380

381

382

383

348 Standardized axis points result in alignments that better reflect the collective impacts of axis

349 direction, not magnitude.

#### 3.3 Alignment and comparison of shape differences

351 Meshes and landmark sets for right valves were mirrored across their commissural plane and

analyzed as operational left valves. This is a reasonable approach for equivalve taxa when

analyzing general shell shape, e.g. of the interior or exterior surfaces, but homologous valves

354 should be used for analyses that include inequivalve taxa as, by definition, their two shapes

differ. Landmark sets were then scaled, rotated, and translated (in that order) under all possible

parameter combinations outlined in the preceding section, totaling 45 alignment schemes.

Landmark coordinate values were scaled by dividing the landmark coordinates by a specimen's

size (e.g. centroid size or volume). Scaled landmarks were then temporarily centered on the

359 centroid of the commissure and then rotated via the respective orientation scheme using

360 Generalized Procrustes Analysis (Morpho:procSym, Schlager 2017); scaling during this step was

explicitly disallowed. Lastly, scaled and rotated landmarks were translated to one of the three

target locations (i.e. the beak or centroids of the commissure semilandmarks or shell points).

Similarity of alignments was quantified using the metric distances between the shapes of interior shell surfaces, which were used to reduce the impact of exterior ornamentation on the differences in general shell shape. Sliding semilandmarks on the commissure and the interior surface of the shell were used to capture 'shape.' Initially, for the commissure, 50 equidistant semilandmarks were placed and the curve's starting point was determined by the orientation scheme (e.g. starting at the semilandmark nearest the beak for the SX-COMM orientation, see details in Supplemental Text §2.3, Figure S5); for the interior surface, semilandmarks were placed at proportionate distances along the dorsoventral and anteroposterior axes of each orientation scheme (5% distance used here, which results in 420 semilandmarks; see details and step-by-step visualization in Supplemental Text §2.3, Figure S3, Figure S4, Figure S5). Mixing the orientations of semilandmarks and rotation axes may be useful for comparing the interaction of growth and anatomical direction with shell shape, but this approach can result in unintuitive. and perhaps unintended, shape differences among specimens. After placement of equidistant semilandmarks, those on the commissure curve were slid to minimize their thin-plate spline bending energy and then used to bound the sliding of the surface semilandmarks (Figure S5; Gunz et al. 2005; Gunz and Mitteroecker 2013; implemented via Morpho::slider3d, Schlager 2017). The final sliding semilandmark set consisted of 430 landmarks (50 points on the commissure plus the 380 points on the surface grid which do not lie on the commissure, i.e. the non-edge points; Figure S5). Landmark coverage analyses may be used at this point to maximize downstream statistical power (Watanabe 2018), but we relied on qualitative assessment of shape complexity and landmark coverage for the simple analyses conducted here.



415

384	For each of the 45 alignments, similarity in shell shape was calculated as the pairwise
385	Euclidean distances of the sliding surface semilandmarks. Identical shapes have a distance of
386	zero. Pairwise distances between shapes for each alignment scheme were normalized by their
387	respective standard deviations, making the distances between specimens comparable across
388	alignments. These normalized pairwise distances were then compared in three ways. First, a
389	permutation-based multivariate analysis of variance (perMANOVA as implemented by
390	geomorph::procD.lm, Adams et al. 2021) was used to model the effects of Procrustes Analysis
391	steps on the scaled pairwise distances between specimens. Each of the 45 rows in the analyzed
392	matrix was a unique Procrustes Analysis treatment, or alignment—i.e. a combination of scaling,
393	rotation, and translation—and each of the 55 columns was a scaled distance between a pair of the
394	eleven specimens. Second, this alignment matrix was scaled and centered and Principal
395	Components Analysis was conducted to visualize the individual and joint effects treatments
396	across alignments (i.e. Figure 4). Third, 'hive diagrams' (see network plots in Figure 5d) were
397	used to compare the scaled pairwise distances of specimens among selected alignments to a
398	reference alignment, where scaling = centroid of commissure, rotation = HL-oHL, translation =
399	centroid of shell commissure.

#### 4. Results and Discussion

- 401 All three Procrustes Analysis steps—translation, scaling, and rotation—significantly affect the
- 402 alignments of shells (Table 1, visualized as clustering of steps in Figure 4). As defined in the
- 403 Methods, quantitative similarity in alignment was determined using the scaled, pairwise
- Euclidean distances among the sliding semilandmarks placed on the interior surface of the shell.
- Treatments within steps (e.g. translation to the beak vs. centroid of the shell) differentiate
- alignments while the effects of other parameters are held constant (p=0.001 for all parameters,
- 407 Table 1). Scaling most strongly differentiates alignments, with rotation and translation having
- smaller effects (see standardized effect sizes as Z scores in Table 1). It follows that the
- 409 differences between alignments are smallest among rotation and translation treatments (i.e. the
- smallest distances between alignments reflected as the lowest Sum of Squares, Table 1, see also
- 411 their clustering in Figure 4), and they increase for treatments of scaling. These metric differences
- among alignments are informative for understanding the impacts of individual steps in Procrustes
- 413 Analysis, but visually comparing the orientations of shells is necessary to understand an
- alignment's fidelity to biological homology and/or analogy.

#### 4.1 Effects of translation

- The choice of translation can change how differences in shell shape are interpreted. Translation
- 417 to the beak, the lone homologous point across the class, allows the comparison of shell shapes
- 418 conditioned on directions of growth from their origins (Figure 5c). *Ensis* can be described as
- being posteriorly elongated compared to *Glycymeris*, or *Pecten* as 'taller' than *Pholas* from the



- beak to the ventral margin. Still, translation to the beak can exaggerate or bias the differences in
- 'pure' shell shape. For example, *Ensis* and *Tagelus* have greater distances between their shapes
- when translated to the beak than to the centroid of commissure semilandmarks (red line in
- 423 Figure 5d.iii). Their offset positions of the beak underlies this difference, which is interesting for
- analyses of growth vs. shape, but the shape of the shell, irrespective of its growth, is arguably the
- 425 primary target of ecological selection (Stanley 1970, 1975, 1988; Vermeij 2002; Seilacher and
- 426 Gishlick 2014). Thus, measuring the morphological similarity of shells for studies of
- ecomorphology, trends in disparity, or evolutionary convergence would be best conducted using
- 428 translation to their respective centroids of the commissure or shell surface (Figure 5a,b); these
- 429 two translations yield very similar alignments given the close proximity of their respective
- centroids (as shown by the pale colors linking specimens in Figure 5d.ii; but note the small offset
- between the two centroids for the more irregularly shaped *Cuspidaria*). In general, it is best
- practice to translate shells to their respective centroids of the commissure semilandmarks or shell
- points when morphological analyses target differences in pure shell shape. Translation to the
- centroid of the commissure is preferred because it incorporates homology into the alignment via
- correspondence of the leading edge of shell growth.

#### 4.2 Effects of scaling

436

449

- 437 Scaling has a large effect on the differences between alignments (see largest Sum of Squares for
- 438 the term in the ANOVA, Table 1). Scaling by volume leaves particularly large residual
- 439 differences in shape; the most voluminous shells are made extremely minute (*Pecten* and
- 440 *Tridacna* in particular, Figure 6c) while the least voluminous shells become the largest
- 441 (Nuculana and Cuspidaria). Scaling to logged shell volume does not alleviate these residual
- 442 differences (results not shown), and, moreover, the aim of this scaling step is to remove the
- 443 isometric relationship of size to shape, not its allometric one. The relative sizes of specimens are
- more similar when scaled to the centroid size of the commissure semilandmarks or the shell
- points (Figure 6a,b). These two sizes are tightly correlated (Figure S6) and thus produce very
- similar alignments (Figure 6d.ii). For comparing differences in overall shell morphology in 3D,
- scaling by the centroid size of shell points would best equalize the isometric differences in size
- among specimens, thus concentrating the remaining differences in morphology to their shapes.

#### 4.3 Effects of rotation

- 450 Of the three Procrustes Analysis parameters, rotation is arguably the most important factor
- defining the biological basis for differences in shell shape. Visually, rotation treatments can
- 452 produce nearly orthogonal orientations of specimens (compare the nearly orthogonal orientation
- of the traditional shell length axis for *Ensis* and *Tagelus* between SX-HL-oHL and SX-COMM,
- 454 Figure 7a,e; also reflected in the deep-red bar linking these two taxa in Figure 7f.v and is spacing
- of specimens on the first two PC axes in Figure S7). Equilateral shells are aligned similarly



456 across rotation treatments (compare orientations of Glycymeris, Pecten, and Tridacna, cf. Ostrea, 457 in Figure 7a-e and the less saturated lines connecting them in Figure 7e.ii-v). Differences in 458 alignments become more pronounced among the more inequilateral shells (seen to a minor extent 459 in Chione relative to Glycymeris and Pecten, but notably in Modiolus, Pholas, Cuspidaria, and *Ensis*). Thus, alignments of inequilateral shells tend to reflect a compromise between the often 460 461 subparallel but not orthogonal orientations of their axes (most clearly seen in the changes to the orientation of *Modiolus*, *Pholas*, and *Ensis* relative to *Glycymeris* and *Pecten* in Figure 7a-f). 462 463 Rotation by sliding semilandmarks on the commissure results in a similar alignment of most 464 shells to the hinge line orientation (pale lines in Figure 7e.v), but the relative shape differences of 465 Modiolus, Ensis, and Tagelus indicate the importance and impact of the beak position. The 466 commissure curve begins at the point nearest the beak, which affects the orientation of the 467 surface semilandmark grid (see Figure S5). Thus, in the SX-COMM treatment, the growth and 468 therefore 'shape' of *Modiolus* and *Ensis* is more similar to the tall-shelled *Ostrea* than either are 469 to the putative, similarly elongate *Pholas* and *Tagelus* (which themselves become more dissimilar in shape owing to the slight offset in their beak positions). Overall, rotation using the 470 471 hinge axis and its orthogonal axis as the pseudo dorsoventral axis is likely the best practice for 472 most analyses of shell shape, as discussed below.

#### 4.4 Practical alignments for bivalve shells

474 The axis-based approach to alignment (Figure 7a-d) is useful both for its ability to 475 encompass broad phylogenetic analyses of shell morphology and for its ability to combine extant and fossil data, the latter known almost exclusively from shells. All shell morphologies should fit 476 477 within this scheme, including those with strong lateral asymmetry (e.g. rudists, see Jablonski 478 2020, and those with calcified tubes or crypts (teredinids and clavagellids, Morton 1985; Savazzi 479 1999, each of which have identifiable valves with anatomical axes—whether to include the tubes 480 and crypts as aspects of shell morphology is a different debate). With increasing phylogenetic proximity, the number of point-based biological homologies is likely to increase, permitting 481 482 more traditional approaches to specimen alignment (Roopnarine 1995; Roopnarine et al. 2008; 483 Márquez et al. 2010; Serb et al. 2011; Collins et al. 2013, 2020; Edie et al. 2022; Milla Carmona 484 et al. First View). These shell-based axes and features (Figure 7a-e) are also useful for incorporating fossil taxa into analyses with extant taxa (Yonge 1954; Cox et al. 1969; Stanley 485 486 1970; Bailey 2009), but aspects of the internal anatomy remain crucial for orientation (Stasek 487 1963a), especially the designation of the anterior and posterior ends. Fortunately, in many cases 488 the anteroposterior axis can be determined from imprints of the soft anatomy on the shell surface 489 (e.g. the pallial sinus) or from other shell features (e.g. siphonal canals, pedal gapes). This 490 necessarily variable and often idiosyncratic approach to defining the direction of anatomical axes 491 may result in more digitization error than seen in traditional point-based geometric 492 morphometrics. However, the impact of that error on analytical interpretations of shape



similarity and variance will depend on the overall scale of shape disparity; for analyses of morphology across the class, the latter is likely to far exceed the former.

495 In biological systems with limited homology in a strict, point-based, geometric sense— 496 and even in those with plenty of it—numerous approaches have been used to align specimens for 497 morphological analysis. A single solution likely does not exist, and comparisons among different methods will be the most powerful approach to testing evolutionary hypotheses (see Bromham 498 499 2016 for the necessity of comparative analyses in historical science). As for most analytical 500 frameworks, comparisons of shell shape will require explicit definition of the alignment scheme and interpretation of any differences within those boundaries. Thus, we cannot declare outright 501 502 that one of these alignment schemes is logically superior, but we do recognize a practical 503 solution that, to us, best reflects the decades of study of shell morphology: alignment via the sagittal axis, hinge line, and its orthogonal line as the pseudo dorsoventral axis (SX-HL-oHL). 504 505 Shell height, length, and width have been the principal measurements for analyzing differences in shape, and long-standing, taxon-specific 'rules' have become entrenched in the literature and 506 507 therefore influence our interpretations of the clade's evolutionary morphology (see discussion in 508 Cox et al. 1969:81–82 and the continued utility of these measurements in Kosnik et al. 2006). 509 The SX-HL-oHL rotation tends to orient shells according to the defined axes of those linear 510 measurements. Of course, precedent need not dictate the course of future work, but here, we find 511 it reasonable to align this 'next generation' of shell shape analyses with the long-standing 512 conventions in the literature, if only for comparative purposes.

#### 513 **5.** Conclusions

- The debate on how to align specimens is still relevant in the current era of morphometry, where
- comparisons of animal form are increasingly accessible in 2D, 3D, and even 4D (Boyer et al.
- 516 2016; Olsen et al. 2017; Pearson et al. 2020). But, no matter how shapes are compared,
- 517 interpretations of their differences or variances should be with respect to an assumed anatomical
- alignment. For comparisons of disparate morphologies, particularly those that lack biological
- 519 homology conducive to point-based landmarking, alignments will likely require non-standard
- 520 approaches so that shape differences do not depend on geometric correspondence alone. In
- bivalves, anatomical axes inferred from taxon-specific features offer a class-wide approach to
- orientation. One set of axes in particular (HL-SX-DVX) coincides with historical approaches to
- 523 their morphometry, while another offers new insight into the relationship between shell shape
- and shell growth (COMM-SX). Either of these solutions are valid in their own way. This
- 525 philosophy of specimen alignment may be particularly relevant to other model systems in
- 526 paleobiology and macroevolution that have accretionary-style growth: gastropods, brachiopods,
- 527 corals, bryozoans, etc.—each with limited point-based landmarks corresponding to biological
- 528 homology.



#### 529 6. Acknowledgments

We thank FMNH and NMNH and their staff for access to the specimens used in this study.

#### **531 7. Funding**

- 532 Supported by National Aeronautics and Space Administration (NNX16AJ34G), the National
- 533 Science Foundation (EAR-0922156, EAR-2049627), and the University of Chicago Center for
- 534 Data and Computing.

#### 535 **8. Data Availability**

- Mesh models, landmark data, and code for reproducing analyses and figures available from
- Zenodo: 10.5281/zenodo.6326531; mesh models also available from Morphosource Project ID:
- 538 000429826 (ARK IDs of specimens in Table S1).

#### 539 9. Authors' contributions

- 540 SME and KSC designed the study, SME performed analyses, all authors contributed to the
- 541 writing.

#### 542 10. References

- Adams, D. C., M. L. Collyer, A. Kaliontzopoulou, and E. K. Baken. 2021: Geomorph: Software
- for geometric morphometric analyses. R package version 4.0. https://cran.r-
- project.org/web/packages/geomorph/index.html
- 546 Allen, J. A., and H. L. Sanders. 1969: *Nucinella serrei* Lamy (Bivalvia: Protobranchia), A
- monomyarian solemyid and possible living actinodont. Malacologia 7:381–396.
- Bailey, J. B. 2009: Shell orientation terminology among the Bivalvia (Mollusca): Problems and
- proposed solutions. Journal of Paleontology 83:493–495.
- 550 Bardua, C., R. N. Felice, A. Watanabe, A.-C. Fabre, and A. Goswami. 2019: A practical guide to
- sliding and surface semilandmarks in morphometric analyses. Integrative Organismal
- 552 Biology 1:obz016.
- Bookstein, F. L. 1991: Landmarks. Pp. 55–87 in Morphometric Tools for Landmark Data:
- Geometry and Biology. Cambridge University Press, Cambridge.
- Borras, A., J. Pascual, and J. C. Senar. 2000: What do different bill measures measure and what
- is the best method to use in granivorous birds? Journal of Field Ornithology 71:606–611.
- 557 Boyer, D. M., G. F. Gunnell, S. Kaufman, and T. M. McGeary. 2016: Morphosource: Archiving
- and sharing 3-D digital specimen data. The Paleontological Society Papers 22:157–181.
- Bradshaw, J. D., and M. A. Bradshaw. 1971: Functional morphology of some fossil
- palaeotaxodont bivalve hinges as a guide to orientation. Palaeontology 14:242–249.
- Bromham, L. 2016: Testing hypotheses in macroevolution. Studies in History and Philosophy of



- 562 Science Part A 55:47–59.
- 563 Carter, J. G., P. J. Harries, N. Malchus, A. F. Sartori, L. C. Anderson, R. Bieler, A. E. Bogan, E.
- V. Coan, J. C. W. Cope, S. M. Cragg, J. R. García-March, J. Hylleberg, P. Kelley, K.
- Kleemann, C. McRoberts, P. M. Mikkelsen, J. Pojeta, W. Skelton, I. Tëmkin, T. Yancey,
- and A. Zieritz. 2012: Illustrated glossary of the Bivalvia. Treatise Online No. 48, Part N,
- Revised, Volume 1, Chapter 31:1–209.
- Carter, R. M. 1967: On the nature and definition of the lunule, escutcheon and corcelet in the Bivalvia. Journal of Molluscan Studies 37:243–263.
- 570 Collins, K. S., J. S. Crampton, and M. Hannah. 2013: Identification and independence:
- Morphometrics of Cenozoic New Zealand Spissatella and Eucrassatella (Bivalvia,
- 572 Crassatellidae). Paleobiology 39:525–537.
- 573 Collins, K. S., S. M. Edie, and D. Jablonski. 2020: Hinge and ecomorphology of *Legumen*
- Conrad, 1858 (Bivalvia, Veneridae), and the contraction of venerid morphospace
- following the end-Cretaceous extinction. Journal of Paleontology 94:489–497.
- 576 Cox, L. R., C. P. Nuttall, and E. R. Trueman. 1969: General features of Bivalvia. Pp. 2–129 in R.
- 577 C. Moore, ed. Treatise of Invertebrate Paleontology. Part N, Mollusca 6, Bivalvia. Vol. 1.
- Geological Society of America & University of Kansas, Boulder, CO & Lawrence, KS.
- 579 Crame, J. A. 2020: Early Cenozoic evolution of the latitudinal diversity gradient. Earth-Science 580 Reviews 202:103090.
- 581 Edie, S. M., D. Jablonski, and J. W. Valentine. 2018: Contrasting responses of functional
- diversity to major losses in taxonomic diversity. Proceedings of the National Academy of
- 583 Sciences U.S.A. 115:732–737.
- 584 Edie, S. M., S. C. Khouja, K. S. Collins, N. M. A. Crouch, and D. Jablonski. 2022: Evolutionary
- modularity, integration and disparity in an accretionary skeleton: Analysis of venerid
- Bivalvia. Proceedings of the Royal Society B: Biological Sciences 289:20211199.
- Fang, Z., and T. M. Sanchez. 2012: Origin and early evolution of the Bivalvia. Treatise Online no. 43: Part N, Revised, Volume 1, Chapter 16:1–21.
- Glover, E. A., and J. D. Taylor. 2013: A new shallow water species of *Nucinella* from the
- Philippines (Bivalvia: Protobranchia: Nucinellidae), member of a tropical seagrass
- 591 chemosynthetic community. The Nautilus 127:101–106.
- 592 Gunz, P., and P. Mitteroecker. 2013: Semilandmarks: A method for quantifying curves and
- surfaces. Hystrix, the Italian Journal of Mammalogy 24:103–109.
- Gunz, P., P. Mitteroecker, and F. L. Bookstein. 2005: Semilandmarks in three dimensions. Pp.
- 595 73–98 in D. E. Slice, ed. Modern Morphometrics in Physical Anthropology. Kluwer
- Academic Publishers-Plenum Publishers, New York.
- Jablonski, D. 2020: Developmental bias, macroevolution, and the fossil record. Evolution &
- 598 Development 22:103–125.

### **PeerJ**

- Jablonski, D., S. Huang, K. Roy, and J. W. Valentine. 2017: Shaping the latitudinal diversity
- gradient: New perspectives from a synthesis of paleobiology and biogeography.
- American Naturalist 189:1–12.
- Jackson, R. T. 1890: Phylogeny of the Pelecypoda: The Aviculidae and their allies. Memoirs of the Boston Society of Natural History 4:277–400.
- Kosnik, M. A., D. Jablonski, R. Lockwood, and P. M. Novack-Gottshall. 2006: Quantifying
- molluscan body size in evolutionary and ecological analyses: Maximizing the return on
- data-collection efforts. PALAIOS 21:588–597.
- Lison, L. 1949: Recherches sur la forme et la mécanique de développement des coquilles des Lamellibranches. Mémoires Institut royal des Sciences Naturelles de Belgique 34:3–87.
- Marin, F., N. Le Roy, and B. Marie. 2012: The formation and mineralization of mollusk shell.
- Frontiers in Bioscience (Schol. Ed.) S4:1099–1125.
- Márquez, F., R. Amoroso, M. Gowland Sainz, and S. Van der Molen. 2010: Shell morphology
- changes in the scallop Aequipecten tehuelchus during its life span: A geometric
- 613 morphometric approach. Aquatic Biology 11:149–155.
- Mikkelsen, P. M., R. Bieler, I. Kappner, and T. A. Rawlings. 2006: Phylogeny of Veneroidea
- 615 (Mollusca: Bivalvia) based on morphology and molecules. Zoological Journal of the
- 616 Linnean Society 148:439–521.
- Milla Carmona, P. S., D. G. Lazo, and I. M. Soto. First View: Ontogeny in the steinmanellines
- 618 (Bivalvia: Trigoniida): An intra- and interspecific appraisal using the Early Cretaceous
- faunas from the Neuquén Basin as a case study. Paleobiology.
- Morton, B. 1985: Adaptive radiation in the Anomalodesmata. Pp. 405–459 in The Mollusca,
- Vol. 10, Evolution. Elsevier.
- Morton, J. E., and C. M. Yonge. 1964: Classification and structure of the Mollusca. Pp. 1–58 in
- K. M. Wilbur and C. M. Yonge, eds. Physiology of Mollusca. Vol. 1. Elsevier, New
- 624 York.
- Olsen, A. M., A. L. Camp, and E. L. Brainerd. 2017: The opercular mouth-opening mechanism
- of largemouth bass functions as a 3D four-bar linkage with three degrees of freedom.
- Journal of Experimental Biology 220:4612–4623.
- Owen, G. 1952: Shell-form in the Lamellibranchia. Nature 170:148–149.
- Pearson, K. D., G. Nelson, M. F. J. Aronson, P. Bonnet, L. Brenskelle, C. C. Davis, E. G. Denny,
- E. R. Ellwood, H. Goëau, J. M. Heberling, A. Joly, T. Lorieul, S. J. Mazer, E. K.
- Meineke, B. J. Stucky, P. Sweeney, A. E. White, and P. S. Soltis. 2020: Machine learning
- using digitized herbarium specimens to advance phenological research. BioScience
- 633 70:610–620.
- Roopnarine, P. D. 1995: A re-evaluation of evolutionary stasis between the bivalve species
- 635 Chione erosa and Chione cancellata (Bivalvia: Veneridae). Journal of Paleontology

636	69:280–287.
637	Roopnarine, P. D., J. Signorelli, and C. Laumer. 2008: Systematic, biogeographic, and
638	microhabitat-based morphometric variation of the bivalve Anomalocardia squamosa
639	(Bivalvia: Veneridae: Chioninae) in Thailand. The Raffles Bulletin of Zoology 18:90-98.
640	Savazzi, E. 1987: Geometric and functional constraints on bivalve shell morphology. Lethaia
641	20:293–306.
642	Savazzi, E. 1999: Borng, nestling and tube-dwelling bivalves. Pp. 205–237 in Functional
643	Morphology of the Invertebrate Skeleton. John Wiley & Sons, Chichester.
644	Scarlato, O. A., and Y. I. Starobogatov. 1978: Phylogenetic relations and the early evolution of
645	the Class Bivalvia. Philosophical Transactions of the Royal Society B: Biological
646	Sciences 284:217–224.
647	Schlager, S. 2017: Morpho and Rvcg – Shape analysis in R: R-Packages for geometric
648	morphometrics, shape analysis and surface manipulations. Pp. 217–256 in G. Zheng, S.
649	Li, and G. Székely, eds. Statistical Shape and Deformation Analysis: Methods,
650	Implementation and Applications. Academic Press, London, UK.
651	Seilacher, A., and A. D. Gishlick. 2014: Morphodynamics. CRC Press, Boca Raton, FL.
652	Serb, J. M., A. Alejandrino, E. Otárola-Castillo, and D. C. Adams. 2011: Morphological
653	convergence of shell shape in distantly related scallop species (Mollusca: Pectinidae).
654	Zoological Journal of the Linnean Society 163:571–584.
655	Stanley, S. M. 1970: Relation of shell form to life habits of the Bivalvia (Mollusca). Geological
656	Society of America Memoirs 125:1–282.
657	——. 1975: Why clams have the shape they have: An experimental analysis of burrowing.
658	Paleobiology 1:48–58.
659	——. 1988: Adaptive morphology of the shell in bivalves and gastropods. Pp. 105–141 in E.
660	R. Trueman and M. R. Clarke, eds. The Mollusca Vol. 11, Form and Function. Academic
661	Press, San Diego.
662	Stasek, C. R. 1963a: Orientation and form in the bivalved Mollusca. Journal of Morphology
663	112:195–214.
664	Stasek, C. R. 1963b: Geometrical form and gnomonic growth in the bivalved Mollusca. Journal
665	of Morphology 112:215–231.
666	Taylor, J. D., and E. Glover. 2021: Biology, Evolution and Generic Review of the
667	Chemosymbiotic Bivalve Family Lucinidae. Series 182, The Ray Society, London, UK.
668	Trueman, E. R. 1964: Adaptive morphology in palaeoecological interpretation. Pp. 45–74 in J.
669	Imbrie and N. D. Newell, eds. Approaches to Paleontology. Wiley, New York.
670	Ubukata, T. 2003: Pattern of growth rate around aperture and shell form in Bivalvia: A
671	theoretical morphological study. Paleobiology 29:480-491.
672	Vermeij, G. J. 2002: Characters in context: Molluscan shells and the forces that mold them.



673	<b>Paleobiology</b>	28.41-54
013	I WICOUIUIUS	<b>2</b> 0.11 21.

- Vermeij, G. J. 2013: Molluscan marginalia: Hidden morphological diversity at the bivalve shell
- edge. Journal of Molluscan Studies 79:283–295.
- Visual Computing Lab ISTI CNR. 2019: Meshlab. https://www.meshlab.net
- Waller, T. R. 1998: Origin of the molluscan class Bivalvia and a phylogeny of major groups. Pp.
- 678 1–45 in P. Johnston and J. Haggart, eds. Bivalves: An Eon of Evolution. Vol. 1.
- University of Calgary Press, Calgary.
- Watanabe, A. 2018: How many landmarks are enough to characterize shape and size variation?
- 681 PLOS ONE 13:e0198341.
- Yonge, C. M. 1954: The monomyarian condition in the Lamellibranchia. Transactions of the
- Royal Society of Edinburgh 62:443–478.
- Yonge, C. M. 1955: Adaptation to rock boring in *Botula* and *Lithophaga* (Lamellibranchia,
- Mytilidae) with a discussion on the evolution of this habit. Quarterly Journal of
- 686 Microscopical Science 96:383–410.
- Zelditch, M. L., D. L. Swiderski, and H. D. Sheets. 2012: Geometric Morphometrics for
- Biologists: A Primer. 2<sup>nd</sup> ed. Academic Press, San Diego, CA.

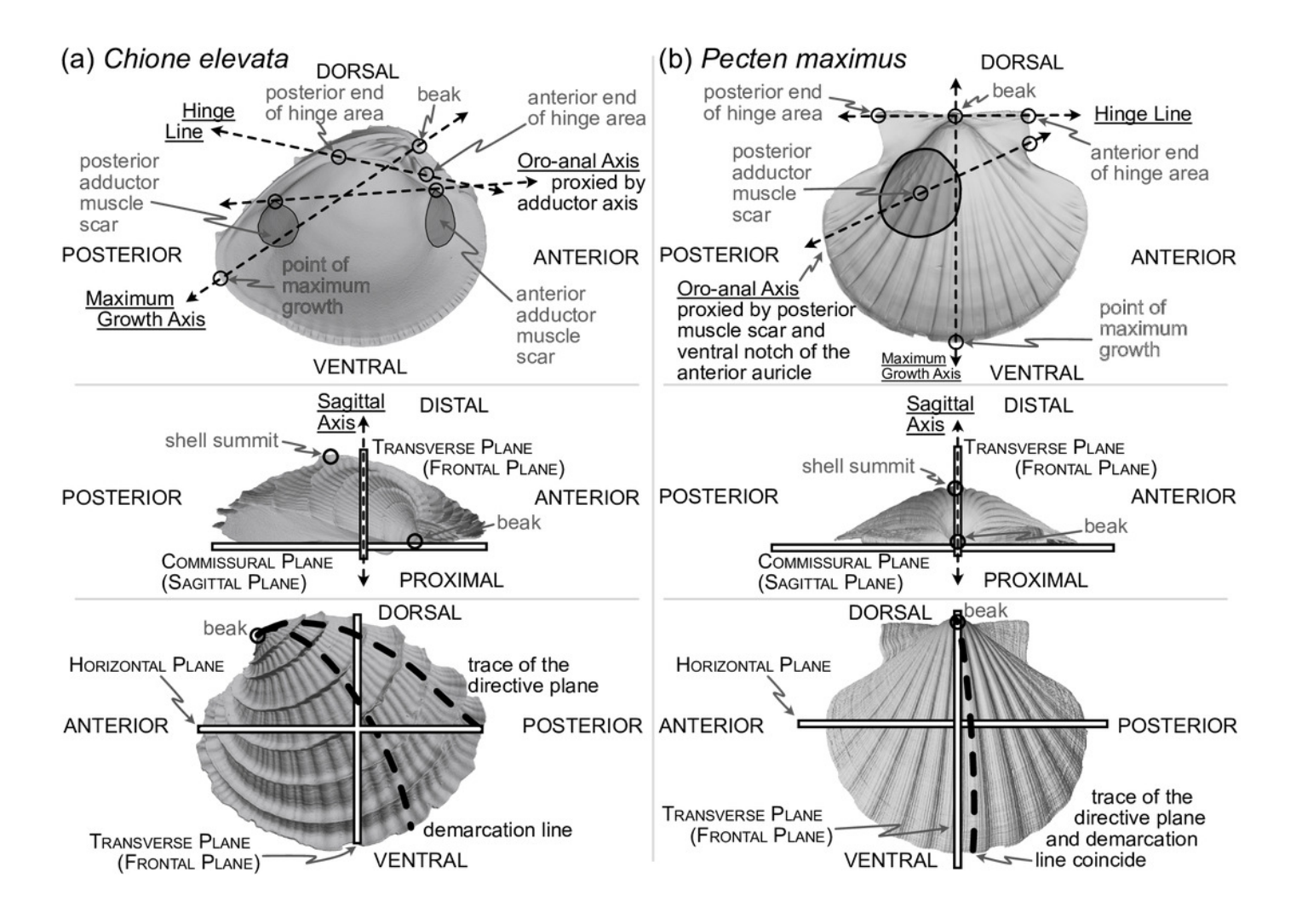
#### 689 9. Table and Figure Captions

- 690 Figure 1. Positions of shell features, axes, and planes as mentioned and defined in text for: (a) a
- 691 helicospiral shell *Chione elevata* (Say 1822), and (b) a more planispiral shell *Pecten maximus*
- 692 (Linnaeus 1767).
- 693 **Figure 2.** (a) Representation of shell commissure curve, its centroid, and the semilandmarks used
- in the COMM orientation scheme. Analyses use 50 sliding semilandmarks on the commissure
- 695 curve, but only a subset is shown here for clarity. (b) Equally spaced points on the shell surface
- placed using a Poisson Disc sampler (Rvcg::vcgSample, Schlager 2017) and their centroid. The
- 697 number and location of vertices on triangular meshes can vary, which strongly influences the
- 698 calculation of centroid size. Analyses use 2000 equally spaced points to minimize this issue
- 699 (only a subset of those points shown here). Figured shell is *Chione elevata*.
- 700 **Figure 3.** Visualization of procedure used to standardize the orientation axes defined by
- 701 landmarks. Figured shell is *Chione elevata*.
- 702 **Table 1.** Permutation multivariate analysis of variance of the scaled pairwise distances between
- 703 specimens across the 45 Procrustes Analysis alignments.
- 704 **Figure 4.** Principal Components Analysis of forty-five alignments (represented by points).
- Spacing of alignments along the first three axes that describe 84.3% of the total variance reflects
- the results of the MANOVA in Table 1. Scaling by shell volume vs. the centroid size of either the
- shell points or the commissure separate along PC1; together, PCs 2 and 3 show the clustering of
- alignments with SX-COMM rotation, translation to the beak, the similarity of translation to the



- 709 centroids of the commissure semilandmarks and shell points, and separation of the axis-based
- 710 rotation schemes.
- 711 **Figure 5.** Effects of translation on differences in shell shapes. All shells are scaled to the
- 712 centroid size of the shell points and rotated using the SX-HL-oHL scheme. For individual images
- of shells, the intersection of the gray line segments marks the origin of the Cartesian coordinate
- system and thus the operational 'center' of the shell. (a) Translation to the centroid of the 2000
- equidistant points placed on the mesh surface of the shell. (b) Translation of shells to the
- centroid of the 50 semilandmark curve along the shell commissure. (c) Translation of shells to
- 717 the apex of the beak landmark, the initial point of shell growth. (d) (i) The scaled pairwise
- 718 Euclidean distances of semilandmarks placed on the interior surface of the shell, scaled to the
- 719 centroid size of the shell points and translated to the centroid of the shell commissure. 'Hotter'
- colors indicate greater relative distances between specimens. (ii-iii) The difference in scaled
- distance of specimens for the specified translation from the reference treatment in panel i. More
- saturated reds indicate an increase in scaled distance relative to the reference alignment;
- 723 conversely, more saturated blues indicate a decrease in distance; white indicates no difference.
- For example, *Ensis* and *Tagelus* become more dissimilar in interior shell shape when translated
- to their respective beaks than when each are translated to their centroid of the commissure.
- 726 **Figure 6.** Effects of scaling on differences in shell shapes. All shells are translated centroid of
- 727 the commissure semilandmarks and rotated using the SX-HL-oHL scheme. Compare differences
- in scaled sizes of specimens across rows, not columns. (a) Shells scaled by the centroid size of
- the 2000 equidistant points placed on the surface of the shell mesh. (b) Shells scaled to the
- centroid size of the 50 semilandmark curve along the shell commissure. (c) Shells scaled by the
- volume of shell carbonate. (d) As in Figure 5d but based on differences in scaling.
- 732 **Figure 7.** Effects of rotation on differences in shell shapes. All shells are translated centroid of
- 733 the commissure semilandmarks and scaled to the centroid size of the shell points. Highlighted
- 734 colors of panel titles correspond to axes plotted on shells. To facilitate relative comparisons of
- shell shape across columns, shells in each row were rotated such that the 'x' axis is parallel to the
- hinge line of *Glycymeris*; this is an ad-hoc, global rotation that does not change between-
- specimen differences in shell shape. (a) Shells rotated by their sagittal axis, hinge line, and
- orthogonal hinge line as the pseudo dorsoventral axis. (b) Shells rotated by their sagittal axis,
- oro-anal axis, and orthogonal oro-anal axis as the pseudo dorsoventral axis. (c) Shells rotated by
- 740 their sagittal, hinge, and maximum growth axes. (d) Shells rotated by their sagittal, hinge,
- 741 maximum growth, and oro-anal axes (e) Shells rotated by their sagittal axis and commissure
- semilandmarks. (f) As in Figure 5d but based on differences in rotation. See Figure S7 for a
- 743 projection of shell shape differences along the first two principal components.

Positions of shell features, axes, and planes as mentioned and defined in text for: (a) a helicospiral shell *Chione elevata*(Say 1822), and (b) a more planispiral shell *Pecten maximus* (Linnaeus 1767).

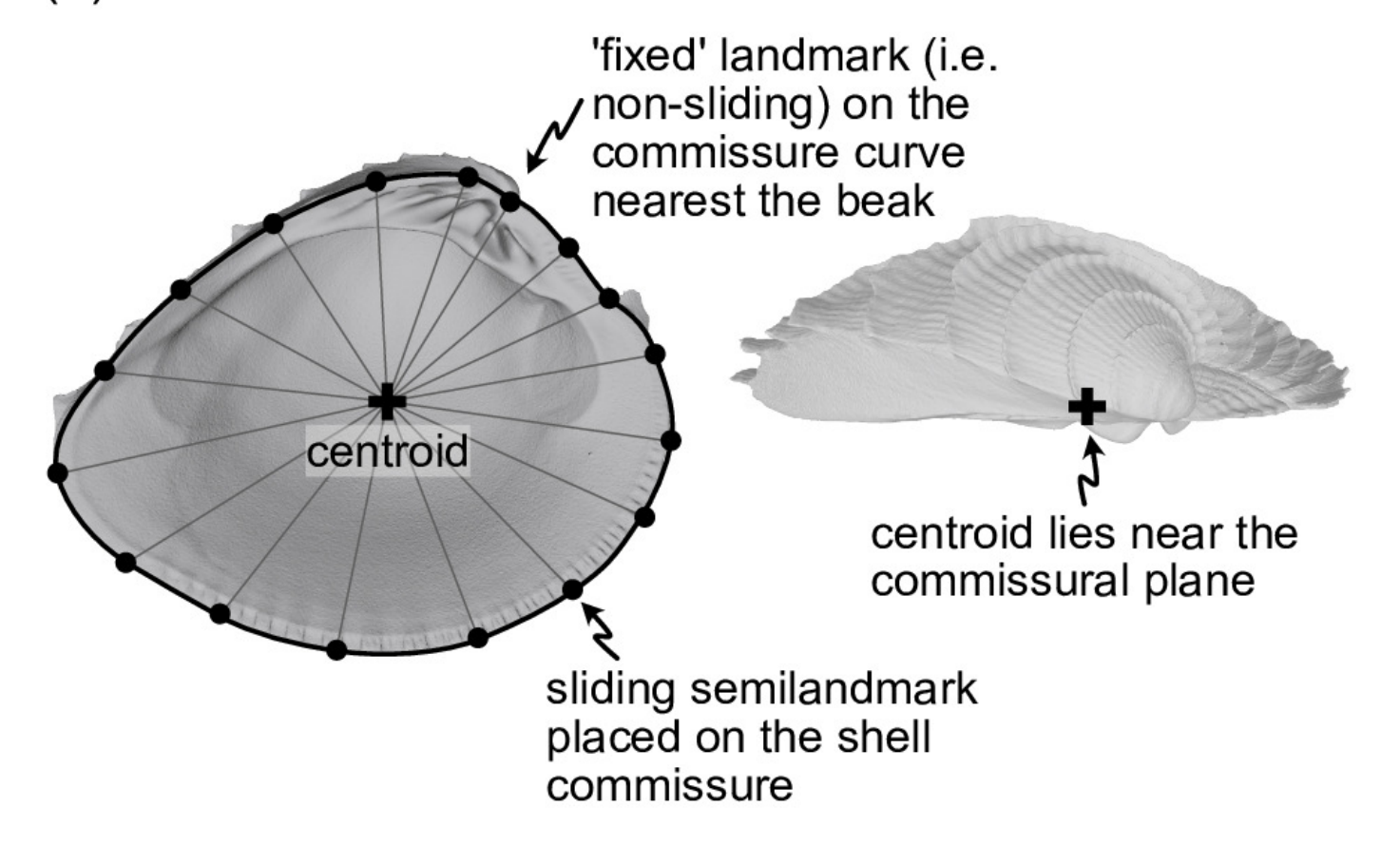




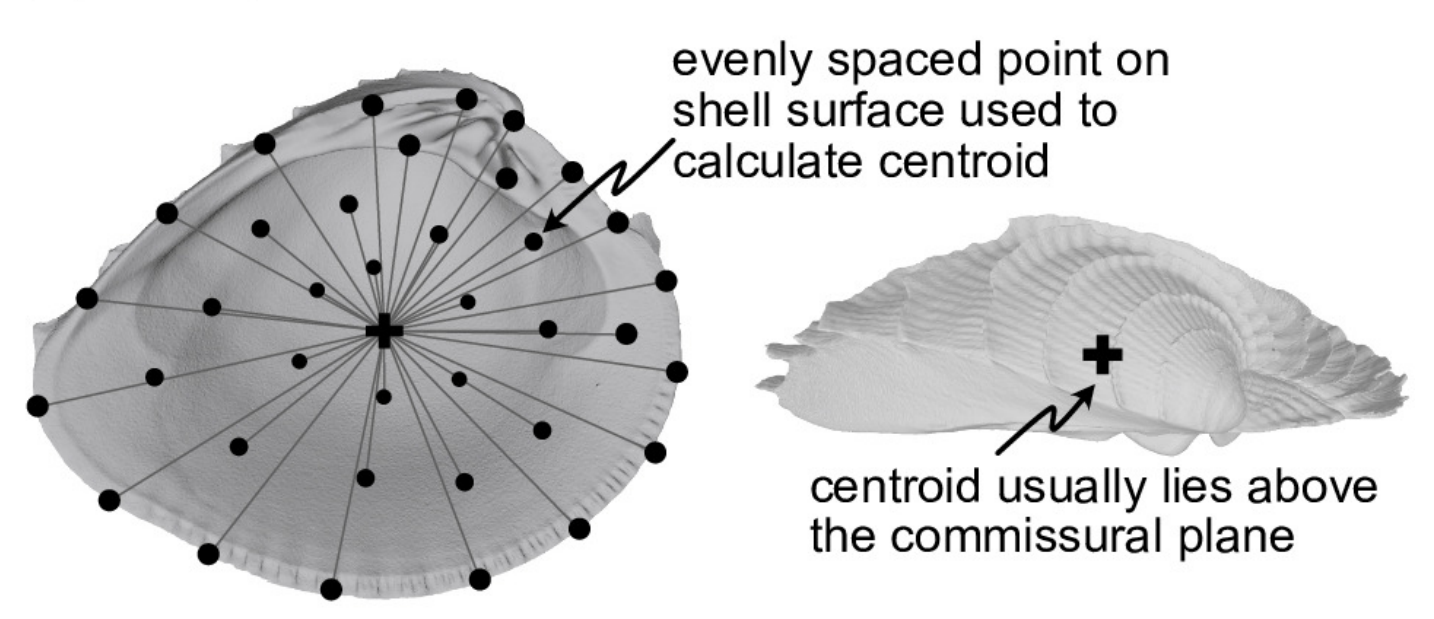
Definition of shell commissure and centroids.

(a) Representation of shell commissure curve, its centroid, and the semilandmarks used in the COMM orientation scheme. Analyses use 50 sliding semilandmarks on the commissure curve, but only a subset is shown here for clarity. (b) Equally spaced points on the shell surface placed using a Poisson Disc sampler (*Rvcg::vcgSample*, Schlager 2017) and their centroid. The number and location of vertices on triangular meshes can vary, which strongly influences the calculation of centroid size. Analyses use 2000 equally spaced points to minimize this issue (only a subset of those points shown here). Figured shell is *Chione elevata*.

### (a) Commissure curve semilandmarks and their centroid



### (b) Shell points and their centroid





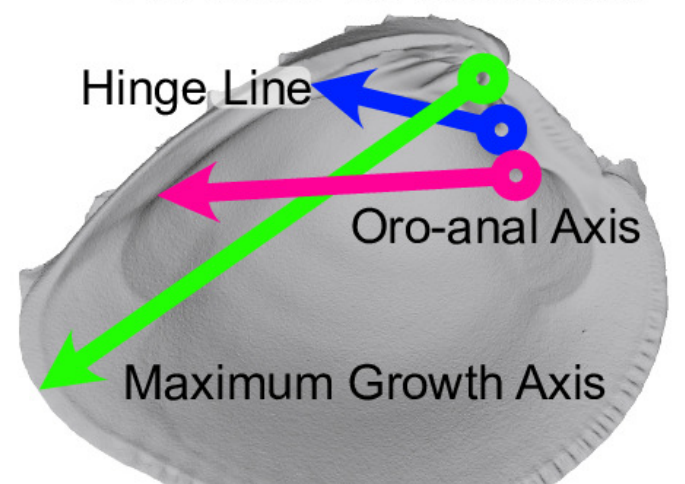
Visualization of procedure used to standardize the orientation axes defined by landmarks.

Figured shell is *Chione elevata*.

# Standardization of axes defined by landmarks

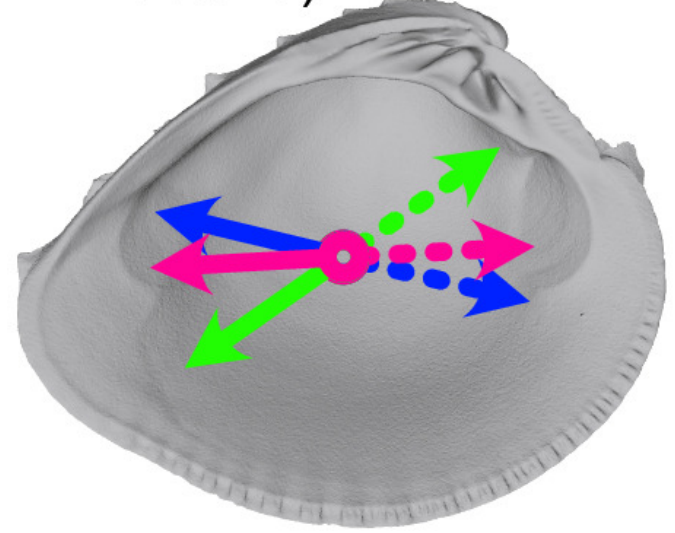
 Landmarks placed to 2. Initial points shifted set axis orientation.

to the centroid of the commissure.



3. Axis 'vectors' normalized to unit length, then duplicated and multiplied by -1 (dashed 'negative' vectors).

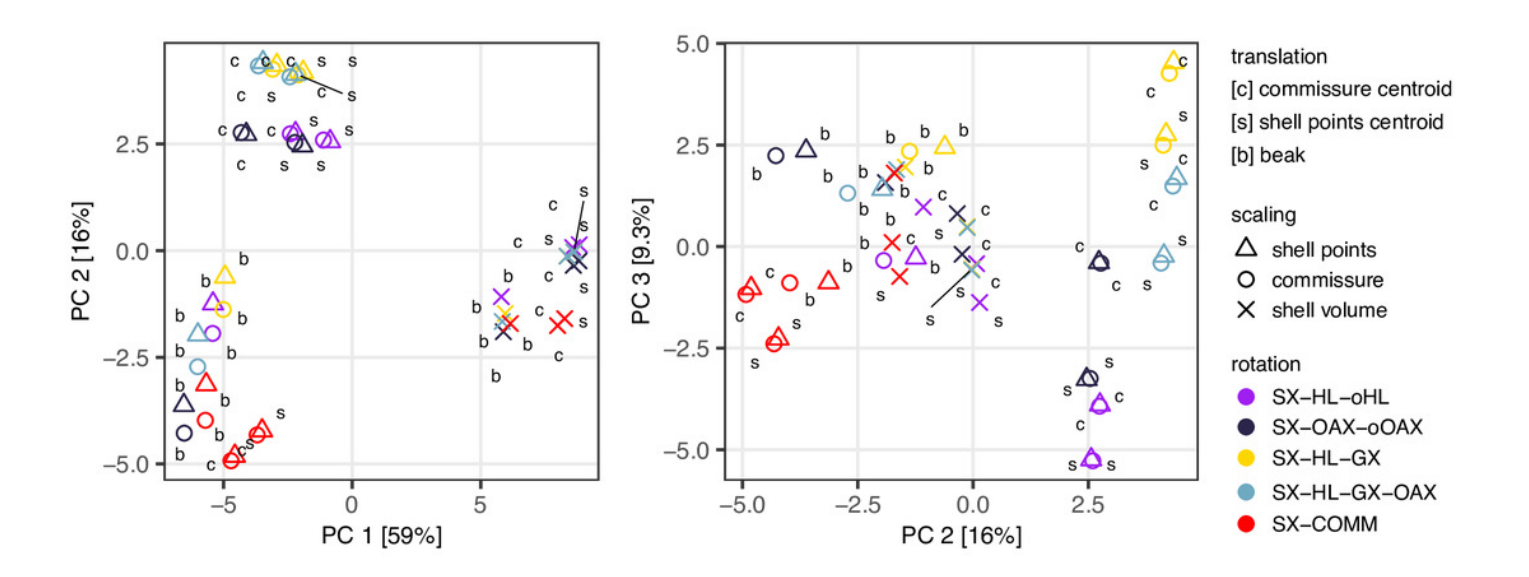
4. Axis 'startpoint' set as the terminal point of the negative vector and axis 'endpoint' set as terminal point of original vector.





Principal Components Analysis of forty-five alignments (represented by points).

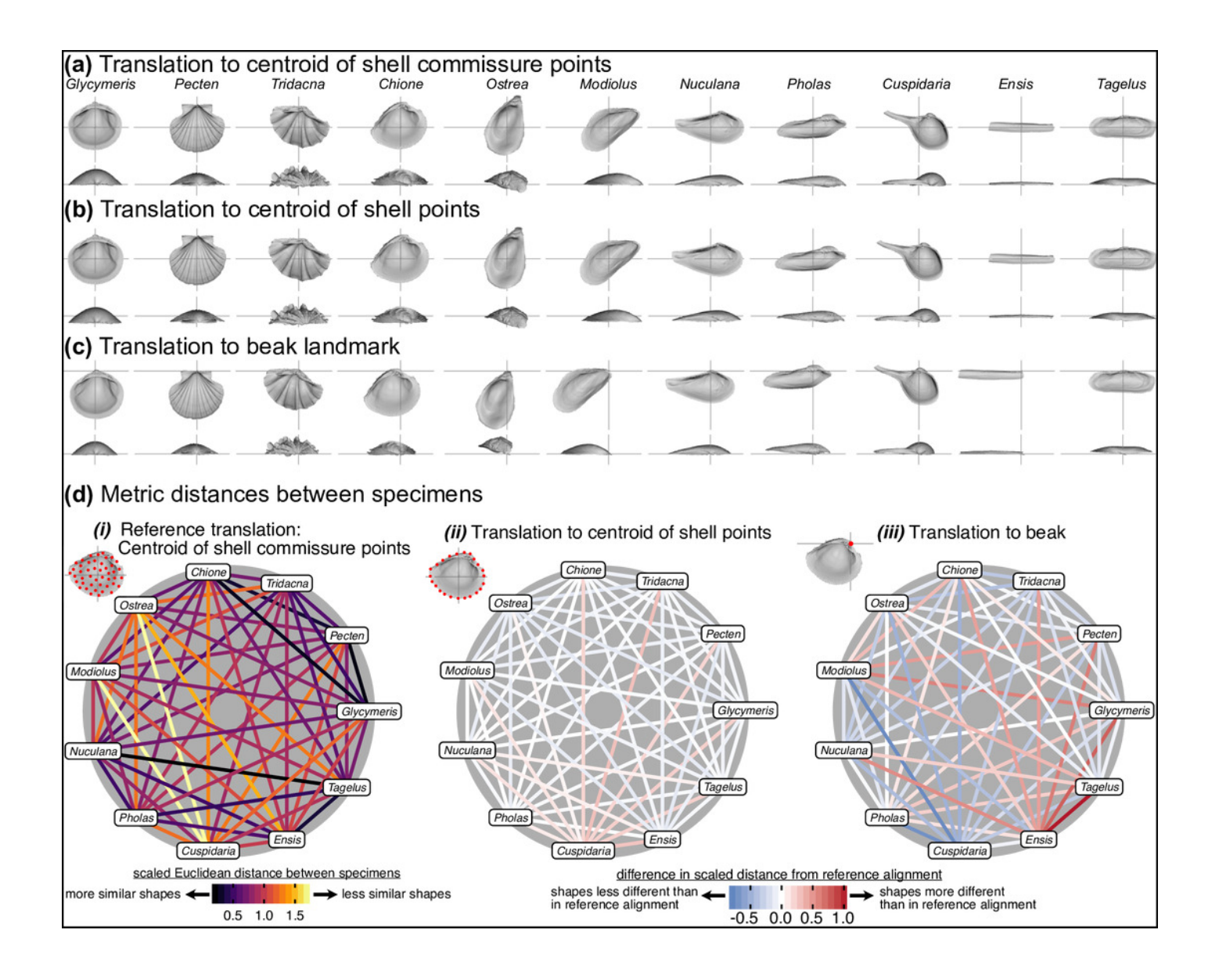
Spacing of alignments along the first three axes that describe 84.3% of the total variance reflects the results of the MANOVA in Table1. Scaling by shell volume vs. the centroid size of either the shell points or the commissure separate along PC1; together, PCs 2 and 3 show the clustering of alignments with SX-COMM rotation, translation to the beak, the similarity of translation to the centroids of the commissure semilandmarks and shell points, and separation of the axis-based rotation schemes.



Effects of translation on differences in shell shapes.

All shells are scaled to the centroid size of the shell points and rotated using the SX-HL-oHL scheme. For individual images of shells, the intersection of the gray line segments marks the origin of the Cartesian coordinate system and thus the operational 'center' of the shell. (a) Translation to the centroid of the 2000 equidistant points placed on the mesh surface of the shell. (b) Translation of shells to the centroid of the 50 semilandmark curve along the shell commissure. (c)Translation of shells to the apex of the beak landmark, the initial point of shell growth. (d) (i) The scaled pairwise Euclidean distances of semilandmarks placed on the interior surface of the shell, scaled to the centroid size of the shell points and translated to the centroid of the shell commissure. 'Hotter' colors indicate greater relative distances between specimens. (ii-iii) The difference in scaled distance of specimens for the specified translation from the reference treatment in panel i. More saturated reds indicate an increase in scaled distance relative to the reference alignment; conversely, more saturated blues indicate a decrease in distance; white indicates no difference. For example, Ensis and Tagelus become more dissimilar in interior shell shape when translated to their respective beaks than when each are translated to their centroid of the commissure.

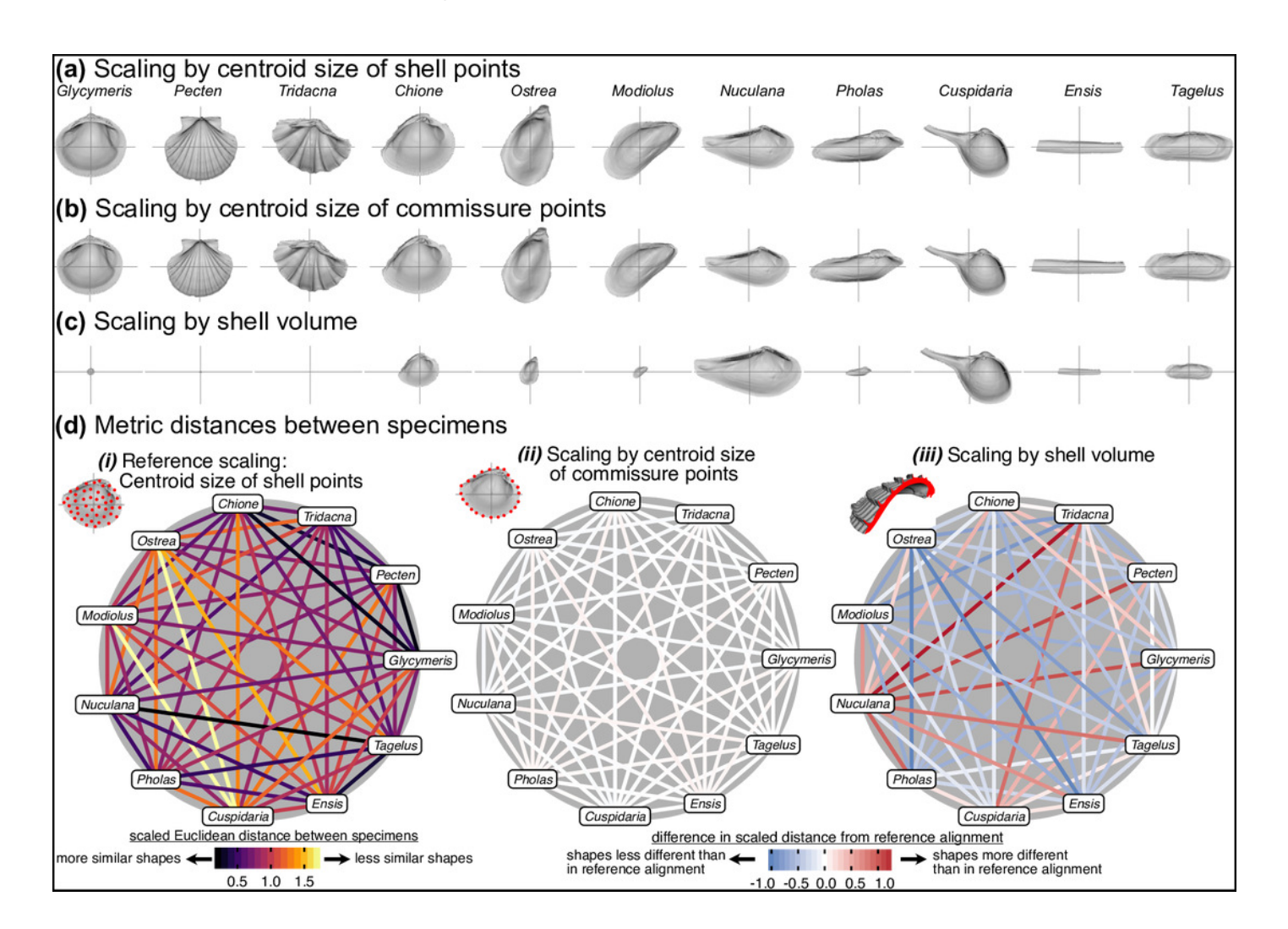






Effects of scaling on differences in shell shapes.

All shells are translated centroid of the commissure semilandmarks and rotated using the SX-HL-oHL scheme. Compare differences in scaled sizes of specimens across rows, not columns. (a) Shells scaled by the centroid size of the 2000 equidistant points placed on the surface of the shell mesh. (b) Shells scaled to the centroid size of the 50 semilandmark curve along the shell commissure. (c) Shells scaled by the volume of shell carbonate. (d) As in Figure 5d but based on differences in scaling.



Effects of rotation on differences in shell shapes.

All shells are translated centroid of the commissure semilandmarks and scaled to the centroid size of the shell points. Highlighted colors of panel titles correspond to axes plotted on shells. To facilitate relative comparisons of shell shape across columns, shells in each row were rotated such that the 'x' axis is parallel to the hinge line of *Glycymeris*; this is an adhoc, global rotation that does not change between-specimen differences in shell shape. (a) Shells rotated by their sagittal axis, hinge line, and orthogonal hinge line as the pseudo dorsoventral axis. (b) Shells rotated by their sagittal axis, oro-anal axis, and orthogonal oro-anal axis as the pseudo dorsoventral axis. (c) Shells rotated by their sagittal, hinge, maximum growth, and oro-anal axes (e) Shells rotated by their sagittal axis and commissure semilandmarks. (f) As in Figure 5d but based on differences in rotation. See Figure S7 for a projection of shell shape differences along the first two principal components.



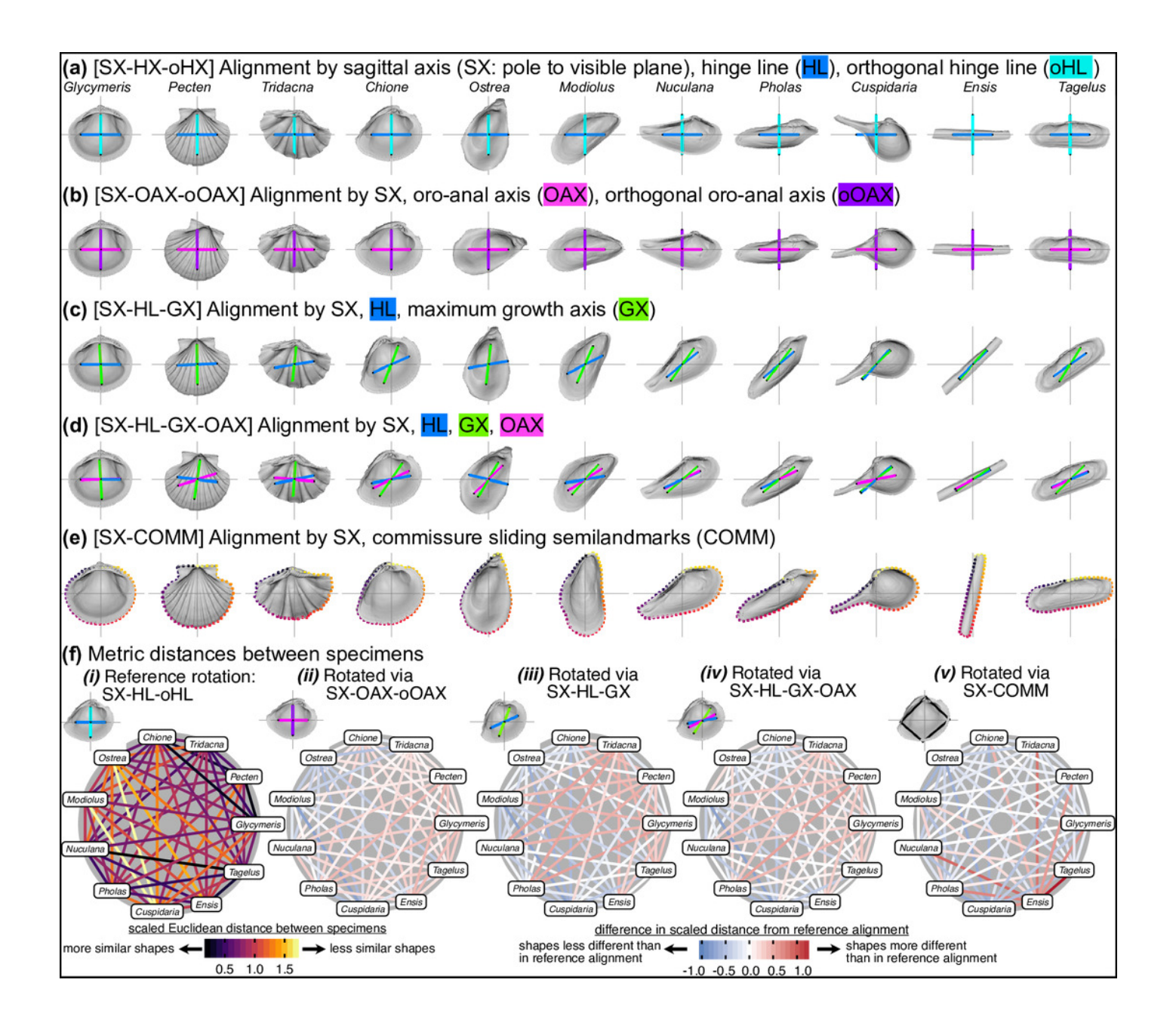




### Table 1(on next page)

Permutation multivariate analysis of variance of the scaled pairwise distances between specimens across the 45 Procrustes Analysis alignments.



Term	df	Sum of Squares	Mean Square	R <sup>2</sup>	F	Z	p
translation	2	30.6	15.3	0.11	13.7	4.4	0.001
scaling	2	185.4	92.7	0.64	82.7	6.2	0.001
rotation	4	34.7	8.7	0.12	7.7	4.8	0.001
Residuals	36	40.3	1.1	0.14			
Total	44	291					